Novel deep learning framework for wideband spectrum characterization at sub-Nyquist rate

Shivam Chandhok[1] · Himani Joshi[1,2] · A. V. Subramanyam[2] · Sumit J. Darak[2]

Abstract

Limited availability and high auction cost of the sub-6 GHz spectrum led to the introduction of spectrum-sharing in 5G networks. This demands base stations with the capability of automatic wideband spectrum characterization (AWSC) to identify available vacant spectrum and parameters (carrier frequency, modulation scheme, etc.) of occupied bands. Since WSC at Nyquist sampling (NS) is area and power-hungry and conventional statistical AWSC performs poorly at a low signal-to-noise ratio (SNR), we propose a novel sub-Nyquist sampling (SNS) based deep-learning framework. It is a single unified pipeline that accomplishes two tasks: (1) Reconstruct the signal directly from the sub-Nyquist samples, and (2) Identify the occupancy status and modulation scheme of all bands. The proposed non-iterative approach based reconstruction provides the occupancy status of all bands in a single forward pass leading to significant improvement in execution time over state-of-the-art iterative methods. In addition, the proposed approach does not need complex signal conditioning between reconstruction and characterization. We extensively compare the performance of our framework for a wide range of modulation schemes, SNR and channel conditions. We show that the proposed framework outperforms existing SNS based characterization and its performance approaches NS based framework with an increase in SNR without compromising computation complexity. A single unified deep-learning framework makes the proposed method a good candidate for reconfigurable platforms.

Keywords Deep learning · Modulation classification · Spectrum reconstruction · Wideband spectrum digitization

✉ Himani Joshi
himanij@iiitd.ac.in

Shivam Chandhok
chandhokshivam@iith.ac.in

A. V. Subramanyam
subramanyam@iiitd.ac.in

Sumit J. Darak
sumit@iiitd.ac.in

[1] IIT-Hyderabad, Hyderabad 502285, India

[2] Electronics and Communications Department, IIIT, Delhi 110020, India

1 Introduction

Sub-6 GHz spectrum is critical for cellular network to support reliable outdoor communication and wide network coverage. Conventional static spectrum allocation policies have led to limited availability of spectrum though various measurement studies showed that sub-6 GHz spectrum is not efficiently utilized [1]. Still, the service operators need to spend billions of dollars each year to access a small licensed spectrum. Limited availability and high auction cost of the sub-6 GHz spectrum led to the introduction of spectrum-sharing in 5G networks, and possible deployment of the cellular network in licensed, shared, and unlicensed spectrum [2]. This demands base stations with the capability of automatic wideband spectrum characterization (AWSC) to blindly estimate the characteristics of the spectrum, such as the location of vacant and occupied bands, interference identification, modulation scheme, along with direction-of-arrival of each band [3, 4]. The AWSC has been discussed widely for military applications

such as electronic warfare, surveillance, signal jamming, and target acquisition [5]. It is also envisioned for next-generation intelligent radios with capabilities such as spectrum sharing [6], channel-dependent rate adaptation [7] and licensed user characterization to avoid the emulation attacks [8] and joint radar-communication systems.

Conventional AWSC demands ultra-high-speed Nyquist rate analog-to-digital converters (ADCs), and computationally intensive filter-bank based channelizers to downsample the desired frequency bands. To reduce the area, power and latency of AWSC, various sub-Nyquist sampling (SNS) methods have been explored, which exploit the sparsity of a wideband spectrum to perform digitization via multiple low-rate ADCs [9, 10]. Such digitized signal is reconstructed to closely match with Nyquist-rate signal followed by spectrum characterization. Existing SNS based AWSC performs sequential characterization by treating wideband spectrum as multiple narrowband frequency bands and deploying various narrowband characterization approaches based on statistical, machine and deep learning methods [11–15]. Such an approach demands complex signal conditioning blocks (like interpolation and filtering blocks) between reconstruction and characterization stages for a wideband spectrum. Such an approach incurs high characterization time and heterogeneous architecture, which is tedious to implement and integrate. From reconfigurability perspective, they offer limited flexibility due to fewer common functions between blocks. Furthermore, the characterization performance of statistical and machine learning-based approaches is poor, especially at low SNR.

To overcome the limitations of the existing AWSC, we propose a novel DL based AWSC framework which is carefully designed as a single unified pipeline and performs two tasks: (1) Reconstruct the wideband spectrum signal sampled using state-of-the-art SNS methods, and (2) Identify the frequency band status and modulation schemes of all active transmissions in the wideband signal. Our main contributions are summarised below:

1. Conventional digital reconstruction of a wideband SNS signal is replaced with a novel DL based approach. Considering the requirement of non-contiguous and reconfigurable SNS where parameters such as the number of bands and sparsity vary with time, the proposed architecture is carefully designed to be agnostic to these parameters.

2. Furthermore, unlike the existing DL based reconstruction [16–18], which employ an iterative procedure to sense a single band at a time, the proposed non-iterative DL based approach senses and reconstructs all bands simultaneously, hence, making it computationally efficient.

3. In terms of reconstruction performance, we show that the proposed reconstruction approach offers better performance than conventional approaches like orthogonal matching pursuit (OMP) approach [19]. In addition, OMP needs sparsity information of the sensed spectrum which is difficult to predict in dynamic environment.

4. We show that the proposed deep learning approach for wideband spectrum sensing and reconstruction offers lower computational complexity and is faster than OMP [19] and DL based OMP methods [16–18].

5. We propose DL based modulation classifier that classifies all signals in the wideband spectrum simultaneously, as compared to sequential single band classification in existing approaches [11–15, 20–24]. Furthermore, the proposed approach is more sophisticated than a Velcro approach of stacking multiple classifiers in parallel. We explore a new formulation of the cross-entropy loss function to classify multiple bands in the wideband signal simultaneously.

6. We develop and share new datasets which are the only publicly available datasets for SNS based AWSC [25]. We extensively compare the performance of our framework for a wide range of modulation schemes, SNR and channel conditions. We show that the proposed framework outperforms existing SNS based approaches and characterization performance approaches to Nyquist sampling based framework with an increase in SNR.

To the best of our knowledge, the proposed unified pipeline of DL framework for AWSC is the first work that combines DL based spectrum status determination, reconstruction and modulation classification from the sub-Nyquist rate samples in a single pipeline. Furthermore, easy to design and integrate due to fewer blocks, along with a single unified DL framework makes it a good candidate for reconfigurable platforms such as Zynq system-on-chip, which is another important aspect of the proposed work.

The rest of the paper is organized as follows. The literature review of existing AWSC methods is discussed in Sect. 2. Section 3 describes the proposed end-to-end pipeline for AWSC. Section 4 discusses the proposed DL based wideband spectrum sensing (DLWSS) followed by the explanation of DL based modulation classification (DLMC) in Sect. 5. The simulation set-up describing the dataset and tool used for DL based AWSC is described in Sect. 6. Performance comparison of the proposed DLWSS and DLMC for AWSC is done in Sect. 7 followed by the Declaration and Conclusions in Sects. 8 and 9, respectively.

2 Literature review

In this section, we review various state-of-the-art approaches involved in AWSC such as digitization, reconstruction and spectrum characterization. Please refer to Fig. 1 for the summary for various approaches in each domain.

2.1 Sub-Nyquist sampling (SNS) approaches

The Nyquist sampling based AWSC demands ultra-high-speed ADCs, which are expensive and power-hungry. Various spectrum occupancy measurements indicated that the spectrum is sparse, and hence, it can be digitized at a fraction of Nyquist rate, f_{nyq}. This led to various SNS approaches using low-speed ADCs such as multi-coset sampling (MCS), modulated wideband converter (MWC) and finite rate of innovation (FRI) [9, 10].

In MCS [9], each of the K low-speed ADCs digitizes a wideband signal with a unique time-offset, and such offset is exploited to reconstruct the wideband signal from SNS samples. However, for ultra-wide spectrum, the offset is of the order of pico-seconds which is difficult to maintain in analog front-end (AFE). Furthermore, analog bandwidth of ADC is still high. The MWC overcomes these limitations with slightly higher complexity in AFE. In MWC, every ADC branch has a unique analog mixer followed by low pass filter and ADC. The unique mixing function aliases all frequency bands at the baseband. Since the bandwidth of the aliased signal is the same as the frequency band bandwidth, $B << f_{nyq}$, the analog bandwidth of the ADC is significantly reduced, i.e. $B\ Hz$. Though conventional MCS and MWC can digitize only contiguous wideband spectrum, FRI based SNS [9, 10], an extension of MWC, overcomes this limitation. As expected, FRI demands

additional intelligence to chose which frequency bands to digitize and needs reconfigurable mixer in AFE. The design and configuration of the proposed AWSC approach are independent of SNS approach compared to [11–15], which used a trivial random sampling.

2.2 Digital reconstruction approaches

After SNS, the next step is to reconstruct the wideband spectrum in the digital domain. Various reconstruction approaches have been explored in the literature. Please refer to [26] for more details. We can broadly classify these approaches into three categories: (1) Greedy algorithms [27], (2) l_1−minimization algorithms [28] and (3) Bayesian algorithms [29]. Among them, the greedy algorithm such as OMP [19] is widely used due to lower computational complexity. From the recently proposed methods that use DL for compressive sensing, [16–18] are closest to our work since they operate directly on the wideband signal as input. To improve the reconstruction performance, [16–18] replace the correlation step of OMP with DL architectures i.e. convolutional deep stacking network (CSDN), multi-layer deep neural network (DNN) and long short term memory (LSTM), respectively, to reconstruct the signal. Similar to OMP, [16–18] follow the iterative approach to determine the status of each band and need prior knowledge of the number of occupied bands. In this paper, we aim to overcome these limitations and propose a method which does not use the aforementioned band-wise iterative approach. Once we train the proposed DL based network, we simply get the occupancy status of all bands simultaneously in one forward pass enabling us to reconstruct the signal.
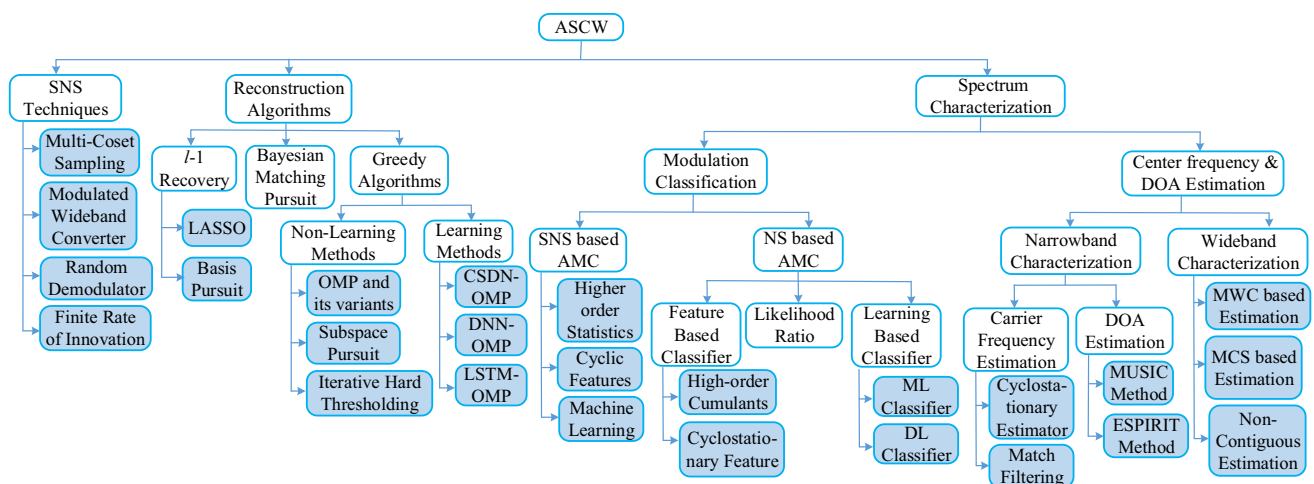

Fig. 1 Various SNS, reconstruction and characterization approaches for automatic wideband spectrum characterization (AWSC)

2.3 Narrow band characterization

As discussed in Sect. 1, the majority of the existing works focus on the narrowband characterization in which complex digital front-end (DFE) involving tunable channelizers are deployed to bring the desired frequency band to the baseband. For characterizing the carrier frequency, cyclostationary estimator, and match filtering are widely studied [30]. Furthermore, for direction of arrival (DOA) estimation, various variants of multiple signal classification (MUSIC) and estimation of signal parameters via rotational invariant technique (ESPRIT) algorithms are developed [31]. Whereas for determining the modulation schemes, various automatic modulation classification (AMC) techniques such as likelihood ratio (LR) based classifiers, feature-based (FB) classifier and intelligent learning (IL) classifiers are studied [32]. LR based classifiers treat AMC as a multiple-composite hypothesis testing problem and parameters are determined by applying the maximum likelihood estimation (MLE) criteria. The drawback of this approach is that the classification accuracy depends on the knowledge of channel and noise model, which varies dynamically in the real environment. To overcome this, FB classification methods are studied. They analyze a variety of statistical features of the received spectrum such as first and second-order moments, cumulants and cyclostationary features. Extensive research has been focused on the usefulness and performance analysis of these methods [32].

Recently, IL based AMC exploiting features along with learning algorithms such as support vector machine (SVM), k-nearest neighbor (KNN), random forest (RF) and neural networks (NNs) [20–24, 32–35] have shown to offer a significant improvement in performance with limited prior knowledge of spectrum. Among them, NNs based AMC are state-of-the-art methods [20–24, 33–35]. NNs are DL models which work as function approximators and extract desirable patterns from the underlying relationships in data. In [20–22] authors adopt the principle architectures used for the task of image recognition for the AMC along with an extensive analysis to study the effect of network depth, filter sizes and the number of filters on the classification accuracy. To determine the modulation scheme, [33] proposed a deep learning framework that converts the input IQ samples into the Contour Stella Image (CSI) and then utilized CSI to perform AMC. But this approach requires an extra overhead of generating CSI. To overcome this drawback, [23, 24, 34, 35] directly utilized the IQ samples for AMC. In [24], a simple convolutional NN (CNN) model with only two layers is used for AMC. The representation of the input signal for DL algorithms is analysed in [23] and it has shown that the use of amplitude-phase samples with LSTM learning algorithm outperforms the

real and imaginary sample based CNN AMC [24]. Also, [24] used different trained models for each SNR, so, for every received signal, [24] would need to first estimate the SNR and apply its corresponding trained model for AMC. [35] overcomes this drawback by jointly training the models of multiple tasks. [35] has created a single trained model for all SNRs under carrier frequency offset and carrier phase offset conditions. The AMC methods discussed in [20–24, 33, 35] perform centralized AMC which might not be suitable for edge devices. To overcome this challenge, distributed AMC is proposed in [34] where multiple edge devices (EDs) send the local weights to one primary edge device (PED). The PED then performs model averaging and sends the averaged weight to the EDs to continue the training process until the convergence of loss function. We would also like to highlight the RadioML dataset [36] is used widely for DL based ASC [23, 24]. However, this dataset along with existing state-of-the-art approaches are suitable only for narrowband AMC with Nyquist rate based digitization. Since there are no comprehensive datasets for wideband characterization using sub-Nyquist samples, we aim to generate such dataset for AWSC.

2.4 Wideband characterization

The extension of narrowband ASC to wideband ASC is non-trivial due to the need for SNS, digital reconstruction, channelization and characterization algorithms and their integration. To characterize the carrier frequency and DOA, [37–39] are the state-of-the-art methods which use MWC, MCS and FRI based joint estimation for AWSC. To the best of our knowledge, [12–15] are the only AMC work which consider AWSC. Their limitations are: (1) They do not consider state-of-the-art SNS approaches, (2) Need tunable channelizers to convert wideband spectrum to multiple narrowband signals for characterization using narrowband methods, and 3) Complex signal conditioning between reconstruction and characterization. We aim to overcome these drawbacks.

3 Proposed AWSC architecture

In this section, we briefly present the proposed end-to-end architecture for AWSC and elaborately discuss the architecture in Sect. 4 and 5. We begin with the assumed received wideband signal model.

3.1 Signal model

Consider a wideband spectrum consisting of a multiple disjoint (i.e. having distinct central frequency) narrowband

signals of maximum possible bandwidth, B Hz. Mathematically, the received wideband signal, $y(t)$ can be modeled as

$$y(t) = \sum_{p=1}^{P} h_p(t) * a_p(t) e^{j2\pi(f_p+f_d)t} + \eta(t) \qquad (1)$$

where P is the maximum possible number of narrowband signals in $x(t)$, $a_p(t)$ is the pth modulated narrowband signal of carrier frequency f_p, $h_p(t)$ is the channel response faced by the pth signal, f_d is the Doppler frequency, $\eta(t)$ is additive white Gaussian noise (AWGN) and $*$ is a convolution operator. The modulated narrowband signal, $a_p(t)$ can be represented as

$$a_p(t) = \sum_{l=1}^{L} g(t - lT_s) b_l^m \qquad (2)$$

where $g(t)$ is the impulse response of a root raised cosine (RRC) pulse shaping filter, T_s is the symbol period, b_l^m is the lth modulated symbol of mth modulation scheme and L is the length of symbol sequence. Similar to [9, 10], we made the following realistic assumptions on the wideband signal:

1. The received wideband spectrum, $Y(f)$, of Nyquist frequency, f_{nyq} is divided into N frequency bands of bandwidth, $B = \frac{f_{nyq}}{N}$.
2. The bandwidth of a narrowband signal $a_p(t)$ does not exceed B Hz.

For the ease of understanding, the frequently used notations are summarized in Table 1.

3.2 AWSC architecture

The proposed AWSC architecture, shown in Fig. 2, can be divided into three sections: (1) AFE for analog signal conditioning, (2) SNS for digitization, and (3) DFE comprising of the proposed DL based reconstruction and characterization.

The main task of AFE is to perform impedance matching, low noise amplification and equalization on the received RF wideband signal, $y(t)$ [40]. For the simplicity of analysis, we assume, the output, $x(t)$, of AFE is approximately same as $y(t)$. Next step is SNS based digitization using multiple low-speed ADCs. As discussed in the Sect. 2, various SNS architectures like MCS and MWC, which can digitize contiguous wideband spectrum and FRI based SNS for non-contiguous spectrum, can be used. The DTFT of sub-Nyquist samples, $z[d]$ can be represented as

$$\mathbf{Z}(f) = \mathbf{A}\mathbf{X}(f) \qquad \forall f \in [0, B] \qquad (3)$$

where $\mathbf{A}$ is a $K \times N$ sensing matrix corresponding to the used SNS architecture and $\mathbf{X}(f)$ contains $X(f - nB)$ as the nth row with $n \in \{1, 2, \ldots, N\}$ and $f \in [0, B]$. Here $K < < N$ is the number of ADCs used in the SNS and N is the number of sensed frequency bands which in case of the contiguous sensing is same as the total number of bands in $x(t)$.

Since the sampling rate of each ADC is $B < < f_{nyq}$, all N frequency bands get aliased at the baseband i.e. in the frequency range of $[0, B]$ as shown in Fig. 2. The aliased sub-Nyquist samples, $\mathbf{Z}(f)$, along with the SNS specific sensing matrix, $\mathbf{A}$ are passed to the proposed DL based AWSC which identifies the vacant bands along with the modulation scheme (BPSK, QPSK, 16-QAM, 64-QAM, 128-QAM, 256-QAM and 8-PAM) of occupied bands. The DL based AWSC consists of three stages: 1) DL based digital reconstruction (DLDR) and 2) (Optional) Symbol Recovery, and 3) DL based modulation classification (DLMC). Various operations in three stages are shown in Fig. 2 and described using Algorithm 1.

The sub-Nyquist samples, $\mathbf{Z}(f)$ and sensing matrix, $\mathbf{A}$ are inputs (line 1) while the occupancy status, $\hat{\mathbf{s}}$ and identified modulation schemes, $\hat{\mathbf{k}}$ of occupied bands are the outputs (line 2). The inputs, $\mathbf{Z}(f)$ and $\mathbf{A}$ are first processed to obtain a pseudo-reconstructed signal, $\tilde{\mathbf{X}}(f)$, (line 3), as

$$\tilde{\mathbf{X}}(f) = \mathbf{A}^{\dagger}\mathbf{Z}(\mathbf{f}) \qquad (4)$$

where $\dagger$ denotes the pseudo-inverse operator. Since $\tilde{\mathbf{X}}(f)$ is a complex signal of dimension $N \times Q$ and can not be feed to the DL model directly, we reshape it to a higher dimensional matrix, $\tilde{\mathbf{X}}_d(f)$ of size $N \times Q \times 2$ (line 4). where the third dimension represents the real and imaginary values of $\tilde{\mathbf{X}}(f)$.


Algorithm 1 Proposed AWSC

1: Input: $\mathbf{A}, \mathbf{Z}(f)$
2: Output: $\hat{\mathbf{s}}, \hat{\mathbf{k}}$
3: $\tilde{\mathbf{X}}(f) \leftarrow \mathbf{A}^{\dagger}\mathbf{Z}(f)$
4: $\tilde{\mathbf{X}}_d(f) \leftarrow \text{Concatenate}(\tilde{\mathbf{X}}_{real}(f), \tilde{\mathbf{X}}_{img}(f))$
5: $\tilde{\mathbf{X}}_n(f) \leftarrow \text{Normalize}(\tilde{\mathbf{X}}_d(f))$
6: $\theta_{ss} \leftarrow DLWSS(\tilde{\mathbf{X}}_n(f), \mathbf{s})$ $\qquad \triangleright$ Training mode
7: $\hat{\mathbf{s}} \leftarrow DLWSS(\tilde{\mathbf{X}}_n(f), \theta_{ss})$ $\qquad \triangleright$ Inference mode
8: $\mathbf{A}_{new} \leftarrow$ Select columns of $\mathbf{A}$ corresponding to occupied bands
9: Determine $\hat{\mathbf{X}}(f)$ according to Eq. 5
10: $\hat{\mathbf{X}}_s \leftarrow$ Symbol Recovery of $\hat{\mathbf{X}}(f)$ $\qquad \triangleright$ Optional Step
11: $\theta_c \leftarrow \text{DLMC}(\hat{\mathbf{X}}_s, \mathbf{k})$ $\qquad \triangleright$ Training mode
12: $\hat{\mathbf{k}} \leftarrow \text{DLMC}(\hat{\mathbf{X}}_s, \theta_c)$ $\qquad \triangleright$ Inference mode

---

For the faster convergence of the training process, the higher dimensional pseudo-reconstructed matrix, $\tilde{\mathbf{X}}_d(f)$ is normalized between [0, 1] (line 5). The normalized matrix, represented by $\tilde{\mathbf{X}}_n(f)$, is fed to DL based wideband spectrum sensing (DLWSS) block. The DLWSS is based on a CNN and its architecture along with the ablation study is

Table 1 Notations and their definitions

Notation	Definitions
$x(t)$	Input to the sub-Nyquist sampling block
b_l^m	l^{th} modulated symbol of mth modulation scheme
T_s	Symbol period
L	Number of modulated symbols for Dataset, $\mathbf{D_{NMC}}$
M	Number of modulation schemes to be classified
N	Number of frequency bands in $x(t)$
B	Bandwidth of a frequency band
f_{nyq}	Nyquist frequency of $x(t)$
$z[d]$	Sub-Nyquist samples of wideband signal $x(t)$
Q	Number of samples/snapshots produced by every ADCs
K	Number of ADCs used for SNS $(K << N)$
W	Number of observations for training DL models
$\tilde{\mathbf{X}}(f)$	Pseudo-reconstruction of $\mathbf{X}(f)$
$\tilde{\mathbf{X}}_d(f)$	Higher dimensional representation of $\tilde{\mathbf{X}}(f)$
$\tilde{\mathbf{X}}_n(f)$	Normalized pseudo-reconstructed signal $\tilde{\mathbf{X}}_d(f)$
$\hat{\mathbf{X}}(f)$	Reconstructed wideband signal
$\hat{\mathbf{X}}_s$	Recovered modulated symbols of a wideband signal, $\hat{\mathbf{X}}(f)$
$\mathbf{s}$	Actual occupancy status of N frequency bands
$\hat{\mathbf{s}}$	Estimated occupancy status of N frequency bands
$\mathbf{A}$	Sensing matrix of size $K \times N$
$\mathbf{A}_{new}$	New sensing matrix of size $K \times \|\hat{\mathbf{s}}\|_0$
$\mathbf{Z}(f)$	Discrete time Fourier transform (DTFT) of $z[d]$
$\hat{\mathbf{k}}$	Estimated modulation schemes of N frequency bands
$\mathbf{p}_{\hat{s}}$	Predicted occupancy probability vector of size $1 \times N$
$\hat{p}_i$	Predicted probability of ith modulation scheme
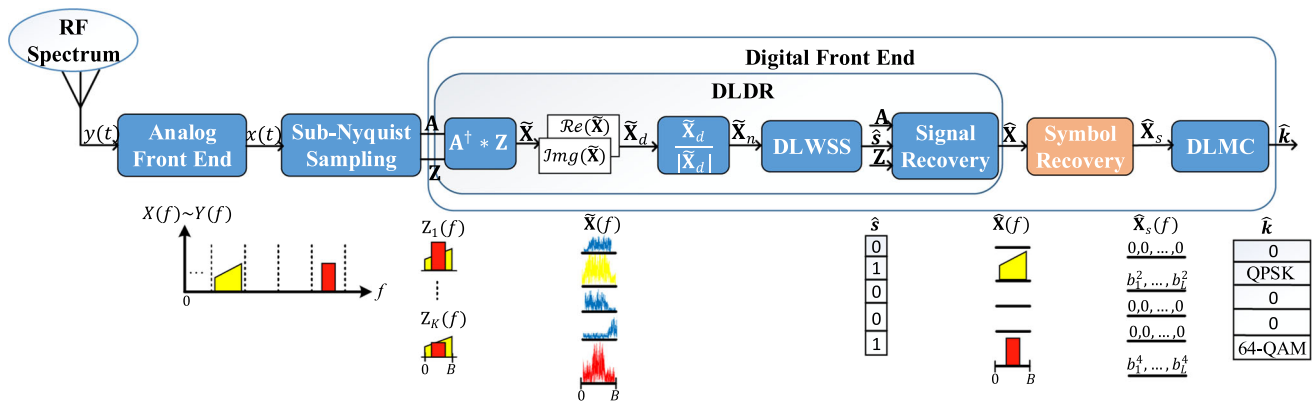
Fig. 2 Proposed deep learning based architecture for end-to-end AWSC

discussed later in Sect. 4. The output of the DLWSS is $\hat{\mathbf{s}}$ which contains the status of each digitized frequency band. Note that $\hat{s}_n = 0 (or 1)$ denotes that n^{th} band is vacant (or occupied).

The DL models work in two modes: (1) Offline training mode and (2) Online inference mode (i.e. testing mode).

Offline training mode provides the learned network parameters, θ_{ss} (line 6) which are then used to determine occupancy status, $\hat{\mathbf{s}}$ (line 7) of bands in the digitized spectrum, $\tilde{\mathbf{X}}_n(f)$. Since the reconstruction noise is very high in the pseudo-reconstructed signal, $\tilde{\mathbf{X}}(f)$, we perform the signal reconstruction (line 8-9) and corresponding

architecture is shown in Fig. 3. Here, we take band occupancy status vector, $\hat{s}$, determined by the DLWSS block, the sub-Nyquist samples, $\mathbf{Z}(f)$ and the sensing matrix $\mathbf{A}$ as inputs. First, we generate a new sensing matrix $\mathbf{A}_{new}$ by selecting the columns of $\mathbf{A}$ which corresponds to the occupied frequency bands (line 8) followed by the reconstruction of wideband signal (line 9). Mathematically, the reconstruction step can be written as

$$\hat{\mathbf{X}}(f) = \begin{cases} \mathbf{A}_{new}^{\dagger}\mathbf{Z}(f) & \text{for occupied bands,} \\ 0 & \text{for vacant bands} \end{cases} \tag{5}$$

where $\hat{\mathbf{X}}(f)$ is the reconstructed wideband signal, $\mathbf{A}_{new}$ is of size $K \times ||\hat{s}||_0$ and $\mathbf{Z}(f)$ is the DTFT of sub-Nyquist samples. For the simplicity of analysis, we refer $\tilde{\mathbf{X}}_n(f), \hat{\mathbf{X}}(f)$ and $\mathbf{Z}(f)$ as $\tilde{\mathbf{X}}_n, \hat{\mathbf{X}}$ and $\mathbf{Z}$, respectively.

After reconstruction, the next step is the modulation classification of all the occupied bands present in the digitized wideband spectrum. As discussed before, we propose simultaneous multi-band classification as opposed to sequential single band classification in existing works [11–15, 20–24]. In this direction, we consider two scenarios:

3.2.1 Scenario 1

In the first scenario, we employ symbol recovery on each occupied band before the modulation classification. The output of this block, as shown in Fig. 2, is represented as $\hat{\mathbf{X}}_s$ and is of size $N \times L$ where L is the number of modulated symbols and b_l^m is the lth modulated symbol of mth modulation scheme. To recover the modulation symbols from $\hat{\mathbf{X}}$, we first perform interpolation on $\hat{\mathbf{X}}$ of every occupied band followed by the root raised cosine filtering. Depending on the requirement, the modulation symbols are represented in one of the two forms: 1) Real and imaginary, and 2) Amplitude and phase. This is followed by the proposed narrowband DL based modulation classifier (NDLMC) that explore a new formulation of the cross-entropy loss function to classify multiple bands in the wideband signal simultaneously, as compared to the sequential single band classification in existing approaches
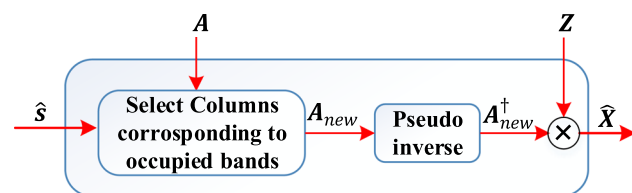
[11–15, 20–24]. Thus, the proposed approach is more sophisticated than a Velcro approach of stacking multiple classifiers in parallel.

3.2.2 Scenario 2

Since the symbol recovery on each occupied band incurs significant computational complexity, we directly characterize the reconstructed wideband signal, $\hat{\mathbf{X}}$ via new wideband DLMC (WDLMC) discussed later in Sect. 5. Another benefit of WDLMC is its architecture similarity with DLWSS making the complete architecture a good candidate for reconfigurable platforms such as Zynq SoC.

4 Proposed DLWSS architecture

The proposed DLWSS is based on the CNN[1]. As discussed in Sect. 2.2, unlike the existing DL based iterative spectrum sensing methods [16–18], which handle single band at a time and involve computing the residual, solving a least squares problem at each iteration until convergence thereby increasing the computational complexity and time, the proposed DLWSS generates the status of all bands simultaneously and does not require any prior knowledge of the sparsity of the spectrum. We choose a CNN for this task since they are good at capturing spatial correlation in input signals which is important for the considered signal model. Furthermore, parameter sharing allows them to operate with a fewer number of parameters enabling the network to be memory efficient and a good candidate for hardware realization.

The CNN architecture for DLWSS and its ablation study are shown in Figs. 4 and 5, respectively. As discussed in Sect. 3.2, we first perform offline training to learn the network parameters, θ_{ss} followed by the testing of real-time pseudo-reconstructed signal in the inference/testing mode. Algorithm 2 shows the offline training process with the dataset, $\mathbf{D}_{WSS} = \{(\tilde{\mathbf{X}}_{n,1}, \mathbf{s}_1), (\tilde{\mathbf{X}}_{n,2}, \mathbf{s}_2), \quad ....., (\tilde{\mathbf{X}}_{n,W}, \mathbf{s}_W)\}$ where W denotes the number of observations (or examples) over which training is performed, $\tilde{\mathbf{X}}_{n,w} \in \Re^{N \times Q \times 2}$ is the wth normalized and pseudo-reconstructed signal, $\tilde{\mathbf{X}}_n$ and $\mathbf{s}_w \in \{0, 1\}^{N \times 1}$ is the label of wth observation indicating the actual occupancy status of all N frequency bands of $\tilde{\mathbf{X}}_{n,w}$ (line 5-7).

Fig. 3 Wideband signal recovery in the DLDR block

---

[1] The CNN is preferred over LSTM based on in-depth study and comparison for a wide variety of DLWSS datasets. The details are skipped due to limited space constraints.
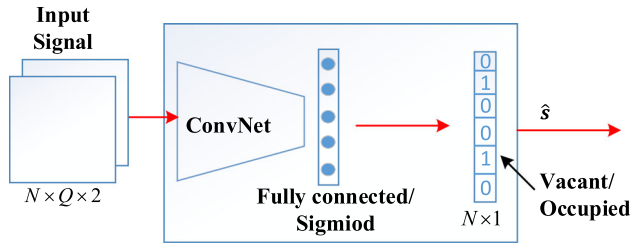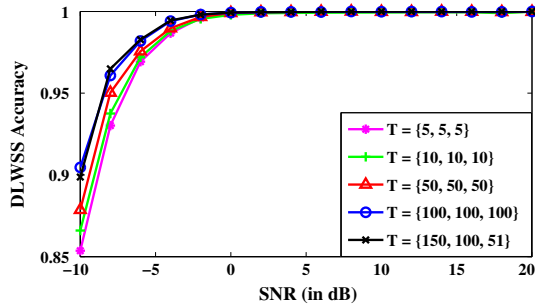
Fig. 4 CNN architecture for DLWSS

Fig. 5 Classification accuracy of CNN based DLWSS for different values of $n - taps$

Algorithm 2 DLWSS Training Mode

1: Input: Dataset= $\{\tilde{\mathbf{X}}_{n,w}, \mathbf{s}_w\} \forall w \in \{1, W\}$, η, $t = 0$
2: Output: θ_{ss}
3: Initialize: $\theta_{ss} = \mathcal{N}(0, 1)$
4: **while** not converge **do**
5:     $t = t + 1$
6:     Sample batch of data-points $\{\tilde{\mathbf{X}}_{n,w}, \mathbf{s}_w\}$
7:     $\hat{\mathbf{s}} \leftarrow CNN(\tilde{\mathbf{X}}_{n,w}, \theta_{ss})$
8:     Calculate L_{BCE} as per Eq. 6
9:     Update θ_{ss} as per Eq. 7
10: **end while**

The training process involves the minimization of a loss function, which is a measure of inconsistency between the predicted and actual label. Since more than one frequency band can be occupied in a wideband spectrum, the problem is formulated as a multi-label binary classification with binary cross-entropy as the training loss function. It is calculated as

$$L_{BCE}(\mathbf{p}_{\hat{\mathbf{s}}}, \mathbf{s}) = -\sum_{n=1}^{N} s(n) \log p_{\hat{s}}(n) + (1 - s(n)) \log(1 - p_{\hat{s}}(n))$$

(6)

where $s(n) \in \mathbf{s}$ is the actual occupancy status of nth frequency band and $p_{\hat{s}}(n)$ is the predicted occupancy probability of nth band (line 8). Furthermore, the learnable network parameters, θ_{ss}, are optimized using a stochastic gradient descent algorithm such that the training loss, L_{BCE}, is minimized. Mathematically, it is represented as

$$\theta_{ss} = \theta_{ss} - \eta \nabla_{\theta_{ss}} L_{BCE}$$

(7)

where η is the learning rate. Here, the loss gradients, $\nabla_{\theta_{ss}} L_{BCE}$ are backpropagated and used to update the learnable network parameters at each iteration (line 9). This process is repeated until the validation loss no more decreases (i.e. until the model converges). The final output is the optimized parameters, θ_{ss}. After the training mode, the CNN model is used in the inference mode to find the occupancy status of unknown wideband spectrum in real-time.

The ablation study of DLWSS CNN model is shown in Fig. 5. The experiments are performed for different network depths and filter setting. The filters used are of the form $1 \times n - taps$ where $n - taps$ denotes the width of the convolution filter in all layers. To perform the ablation for filter size, we fix the number of filters to 64 in all layers. We observe that filters with a larger width perform better as compared to those with a smaller width and saturates when the width is increased further. The same has been shown in Fig. 5 for three-layer CNN. Here, T tells the $n - taps$ values for the three layers of CNN. The best classification accuracy is obtained when $T = \{150, 100, 51\}$. Furthermore, we then fix the filter sizes to the best case and vary the number of filters in each layer. The best performing CNN architecture is shown in Table 2. The same architecture has been selected for the rest of the discussion.

5 Proposed DLMC architecture

As discussed in Section 3, to perform DLMC, we consider two scenarios: (1) NDLMC, and (2) WDMLC. We present the corresponding architectures below.

5.1 NDLMC architecture

As shown in Fig. 2, the output of DLDR block, $\hat{\mathbf{X}}$, is processed via symbol recovery to obtain $\hat{\mathbf{X}}_s$ of size $N \times L$. To perform AMC on this processed baseband spectrum, three types of datasets have been considered in the

Table 2 CNN Architecture for the proposed DLWSS

Layers	Filter Size	Number of Filters	Output Dimension
Input	–	–	$N \times Q \times 2$
Conv/relu	1x150	256	$N \times 150 \times 256$
Conv/relu	1x100	128	$N \times 51 \times 128$
Conv/relu	1x51	64	$N \times 1 \times 64$
Custom pool	–	–	$N \times 1 \times 64$
FC/sigmoid	–	–	N

literature: (1) IQ (in-phase and quadrature-phase) samples [20–22, 24], (2) AP (amplitude-phase) samples [23], and (3) Constellation diagram images of modulation schemes [33, 41]. Since the received wideband spectrum is represented using complex samples, IQ and AP datasets are readily available in the wireless receiver without the need of additional processing in physical layer compared to the constellation image based processing. Hence, we restrict the discussion to IQ and AP samples of $\hat{\mathbf{X}}_s$. Furthermore, our models are designed considering the various studies which show that the CNN and LSTM models are more suited for IQ and AP samples, respectively, [11, 20–24].

Algorithm 3 shows the steps involved in the training of NDLMC. Inputs to this classifier are $\hat{\mathbf{X}}_s$ and the labels of modulation schemes, $\mathbf{k}_w$. Since M modulation schemes are considered for the classification for each of the N frequency bands, the output of the classifier is a vector, $\hat{\mathbf{h}}$ of unnormalized log probabilities and has the size of $1 \times M$. The values in vector $\hat{\mathbf{h}}$ are converted to probabilities by applying a softmax activation function which, for a particular band is calculated as

$$\hat{p_i} = \mathbf{softmax}(\hat{h_i}) = \frac{exp(\hat{h_i})}{\sum_j exp(\hat{h_j}))} \tag{8}$$

where $\hat{p_i}$ is the predicted probability of ith modulation scheme for a frequency band. Thus for all N bands, this gives an output vector of size $N \times M$ (line 5-7). Next, similar to the CNN modeling for DLWSS, to optimise the network learnable network parameters for the modulation scheme classifiers, we use a stochastic gradient descent algorithm to minimize the training loss. As the training loss for a particular frequency band depends on the status of the band, we define it as the categorical cross entropy if the band is occupied and zero if the band is vacant. Mathematically, loss of the nth frequency band can be defined as

$$L_n = \begin{cases} -\sum_i p_i log(\hat{p_i}) & \text{if } \hat{s}_n = 1, \\ 0 & \text{if } \hat{s}_n = 0 \end{cases} \tag{9}$$

where $\hat{s}_n$ is the estimated occupancy status (i.e. 0 for vacant and 1 for occupied) of the nth band, and p_i and $\hat{p_i}$ are the actual and predicted probability of the ith modulation scheme for the nth frequency band.

To determine the complete loss function (line 8), we concatenate the estimated band status vector, $\hat{s}$ with the detected modulation scheme vector, $\hat{\mathbf{k}}$, and it can be expressed as

$$L_c = \sum_{n=1}^{N} -\hat{s}_n \left(\sum_i p_i \log \hat{p_i} \right) \tag{10}$$

where $\hat{s}_n \in \hat{\mathbf{s}}$. Now, similar to DLWSS, the network learnable parameter, θ_c, is updated as (line 9)

$$\theta_c = \theta_c - \eta \nabla_{\theta_c} L_c \tag{11}$$

Algorithm 3 NDLMC Training Mode

1: Input: Dataset= $\{\hat{\mathbf{X}}_{s,w}, \mathbf{k}_w\} \forall w \in \{1, W\}$, η, $t = 0$
2: Output: θ_c
3: Initialize: $\theta_c = \mathcal{N}(0, 1)$
4: **while** not converge **do**
5:     $t = t + 1$
6:     Sample batch of data-points $\{\hat{\mathbf{X}}_{s,w}, \mathbf{k}_w\}$
7:     $\hat{\mathbf{k}} \leftarrow \text{Classifier}(\hat{\mathbf{X}}_{s,w}, \theta_c)$
8:     Calculate L_c as per Eq. 10
9:     Update θ_c as per Eq. 11
10: **end while**

Next step is to finalize the architectures of CNN model. Since the proposed NDLMC is the first work which handles simultaneous classification of multiple bands of a wideband signal in a single forward pass, we perform ablation study to decide the NDLMC architecture.

To start with ablation study, we first establish a simple baseline CNN model (referred as $CNN_{Baseline}$) and discuss it in detail. As the proposed NDLMC aims to simultaneously classify all bands in the multiband input, we need deeper and more complex architectures to capture spatial correlation in the signal. However, deeper models result in vanishing gradients making it difficult for the network to learn optimal parameters. Thus, in addition to $CNN_{Baseline}$, we analyse four approaches namely : (1) Network in Network(NiN) [42], (2) Inception network [43], (3) Residual network (ResNet) [44], and (4) Densenet network [45], to enhance the AMC performance. These models enable us to better capture spatial correlation which is integral for simultaneous multiband classification. Also, they alleviate the gradient vanishing issues to a large extent allowing us to train deeper models. Note that in the proposed setup, the final outcome is of the form $N \times (M + 1)$ comprising of the status of N bands and modulation schemes of occupied bands.

The $CNN_{Baseline}$ architecture is shown in Table 3. We studied the classification performance to decide our baseline model architecture for different sizes of filter (i.e. $n - taps$), number of filter and depth of the network. Fig. 6 (a) shows the classification performance for various values of $n - taps$. We notice that smaller filters (i.e. for $n - taps = 3, 5$) perform better than the larger filters. This is an important observation as it is not valid in case of WDLMC discussed later. Thus, we use small filter sizes $n - taps = 3$ in the $CNN_{Baseline}$. Furthermore, the results obtained by varying the number of filters are very similar to the ones obtained in [22]. Thus, 64 number of filters is considered for further analysis as it is efficient from both computation, memory and performance point of view. Also, as shown in Fig. 6 (b), we observe no significant performance

Table 3 $CNN_{Baseline}$ Architecture for NDLMC

Layers	Filter Size	Number of Filters	Output Dimension
Input	–	–	$N \times L \times 2$
Conv/relu	1×3	64	$N \times L \times 64$
Conv/relu	1×3	64	$N \times L \times 64$
Conv	1×1	$M + 1$	$N \times L \times (M + 1)$
Custom pool/softmax	–	–	$N \times (M + 1)$
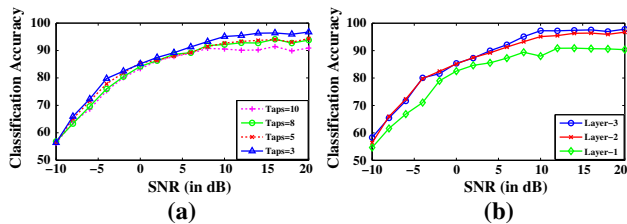
Fig. 6 Ablation study for $CNN_{Baseline}$ on IQ samples for different values of **a** $n - taps$, and **b** Layers

improvements when we increase the number of layers with 1×3 filters beyond 2. Hence, the $CNN_{Baseline}$ has two convolution layers with 1×3 filter size, a convolution layer of filter size 1×1, and a custom average pool/softmax activation layer at the end. The last convolution layer of filter size 1×1, along with the custom pool layer aim to match the dimension of the output label (i.e. $M + 1$) and it is performed by averaging the input along the column dimension (i.e. L). Note that the softmax activation layer associates the output with the probability of occurrence of every modulation scheme.

Next, we extend the proposed baseline model for NiN [42], Inception network [43], ResNet [44], and Densenet network [45] and their performance analysis for different channel conditions, i.e. AWGN, Rayleigh and Rayleigh with a Doppler shift of 10 Hz is shown in Table 4. It can be observed that Inception offers better performance than other architectures, and hence, it is chosen for the NDLMC task with IQ-samples as input. Note that the performance of NDLMC improves if Nyquist sampling is used. Table 5 and Fig. 7 show the corresponding architecture of Inception model for NDLMC and Inception block. In addition to the CNN architecture, we also design a novel LSTM based architecture for NDLMC which similar to the proposed CNN based NDLMC, can handle and simultaneously classify various bands of a multiband. The proposed LSTM based NDLMC architecture with ablation study and the performance analysis is discussed in Appendix A due to space constraint.

Note that since both the proposed CNN and LSTM models employ weight sharing and do not use any special

training strategy for optimization other than the proposed multiband classification loss, the proposed NDLMC method has time and computational complexity comparable to any other recently single band classification models at training and test times both [20–24].

5.2 WDLMC architecture

Next, we consider AMC of the wideband spectrum directly from the reconstructed wideband signal, $\hat{\mathbf{X}}$ (i.e. raw samples). The training of the WDLMC follows the same approach as that of NDLMC in algorithm 3 except that $\hat{\mathbf{X}}$ is used instead of $\hat{\mathbf{X}}_s$ in Line 1. In the end, we have estimated network learnable parameters, θ_c via steepest descent method (line 8-9). To decide the architecture for CNN classifier for WDLMC, we conduct ablation study as shown in Fig. 8. We further design the architecture such that it is similar to DLWSS architecture enabling the proposed model well-suited for realization on the reconfigurable hardware. The chosen WDLMC architecture is given in Table 6. Note that the additional convolution layer of filter size 1 in the architecture is to match the output of the model to the dimensions of the ground truth label which is $N \times (M + 1)$.

The performance of WDLMC for different wireless channels is shown in the last rows of Table 4 along with its performance for Nyquist sampled data. Notice that the performance of the proposed architecture for Nyquist and sub-Nyquist sampled data becomes almost identical as SNR increases showing the strength of the proposed signal reconstruction and classification methodology. As expected, the performance of WDLMC is lower than NDLMC, especially for wireless channels with Rayleigh and Rician fading. This indicates that the design of WDLMC architectures for these channels is itself a challenging research problem. This problem is important for architecture perspective as the design of intelligent and reconfigurable physical layer is one of the critical research areas. In this direction, the significant similarity between our proposed WDLMC and DLWSS architecture in terms of number of layers, number of filters and size makes the proposed AWSC transceiver well-suited for realization on the reconfigurable hardware. For example, via dynamic partial

Table 4 Modulation classification accuracy of various variants of CNN model for NDLMC and WDLMC

DLMC Methods	Classifiers	AWGN					Rician fading with doppler					Rayleigh fading with doppler				
		$-10dB$	$-6dB$	$0\,dB$	$4\,dB$	$14\,dB$	$-10dB$	$-6dB$	$0\,dB$	$4\,dB$	$14\,dB$	$-10dB$	$-6dB$	$0\,dB$	$4\,dB$	$14\,dB$
NDLMC	Baseline	56.4	72.3	85.1	89.2	96.4	45.4	59.3	72.6	74.7	77.1	43.2	58.7	71	71	76.8
	NiN	58.4	72.3	84.5	91.7	99.9	45.1	59.7	72.9	78.1	89.1	44.02	59.4	74.1	79.1	89.6
	ResNet	58.5	72.9	84.6	91.4	99.9	45.9	61.6	74.5	79.1	89.7	46.2	61.2	73.4	79	89.1
	Densenet	57.1	72.9	85.3	90.2	99.8	46.8	61.8	75.9	79.8	90	45.8	60.9	73.5	79	90
	Inception-SNS	**59**	**73.7**	84.4	**91.7**	99.8	**47.5**	**62.3**	**74.8**	**79.8**	89.4	**45.3**	**61.6**	**73.4**	**78.5**	**90.3**
	Inception-NS	68.6	81.5	90.1	97.7	100	54.6	68.3	79.5	86	93.5	57.2	68.6	78.3	83.3	91.1
WDLMC	CNN-SNS	42	49.7	67.1	75.4	82.7	34.8	39.7	45.9	52.6	52	34.3	37.9	42.1	46	47.7
	CNN-NS	43.8	58.1	74.5	79.1	83.2	34.4	44.7	50.2	51.5	53.2	33.1	42.1	45.4	47.8	48.3

reconfiguration capability of Zynq SoC, on-the-fly switch between DLWSS and WDLMC can offer a significant reduction in area and power complexity along with cost benefits due to the reduction in the chip area. Thus, the proposed WDLMC approach is a novel state-of-the-art contribution in the design of reconfigurable AWSC.

Similar to NDLMC, we also show the performance of the proposed LSTM based WDLMC architecture for completeness of the performance analysis and corresponding details are given in Appendix B.

6 Simulation setup

In this section, we discuss the proposed datasets for training and verification of DLWSS and DLMC. The proposed datasets are generated synthetically using MATLAB and are the only available datasets for SNS based AWSC. Each dataset is keyed with modulation scheme and SNR. We consider seven widely used modulation schemes (BPSK, QPSK, 16-QAM, 64-QAM, 128-QAM, 256-QAM, 8-PAM) and SNR ranging from -10dB to 20dB with an interval of 2dB. We consider $N = 14$ frequency bands and MCS based SNS for digitization consisting of 7 ADCs and hence, has a compression ratio of 0.5. For every characterization, we take $Q = 299$ samples from each ADC. To ensure the considered datasets resemble real world conditions and our model can generalise well to different channel variations, we consider various versions of datasets for Rayleigh and Rician fading channels with a Doppler shift of 10 Hz. Next, we explain the details of the dataset. All datasets are free and available online at [25].

6.1 D_{WSS}: DLWSS dataset

The $\mathbf{D}_{WSS}$ dataset is generated using the complex-valued normalized pseudo reconstructed signal, $\tilde{\mathbf{X}}_n$ of size $N \times Q \times 2$. For generating this dataset, real and complex parts of $\tilde{\mathbf{X}}$ are separated and then normalized in the range [0, 1] as shown in Fig. 2. Since this dataset is used for spectrum sensing, the label, $\mathbf{s}$ of each frequency band will either be vacant (i.e. $s_n = 0$) or occupied (i.e. $s_n = 1$).

6.2 D_{NMC}: NDLMC Dataset

The $\mathbf{D}_{NMC}$ dataset uses $\hat{\mathbf{X}}_s$ which is generated by passing the reconstructed wideband signal via symbol recovery. It is different compared to [23, 24] where single frequency band is considered compared to 14 bands simultaneously in our dataset depicting real wideband spectrum based AWSC. Thus, the label, $\hat{\mathbf{k}}$ is of size $N \times 1$ where its nth entry, $\hat{k}_n \in \{0, 1, ..., M\}$. Here, $\hat{k}_n = 0$ denotes that n^{th}

Table 5 Architecture of Inception model for NDLMC

Layer	Output dimension
Input	$N \times L \times 2$
Inception Block	$N \times L \times 192$
Inception Block	$N \times L \times 192$
1×1 Conv/Relu	$N \times L \times (M+1)$
Custom pool/softmax	$N \times (M+1)$
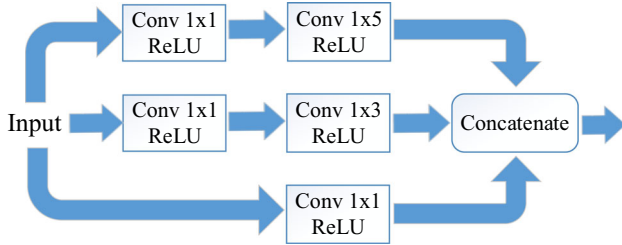
Fig. 7 Architecture of Inception block
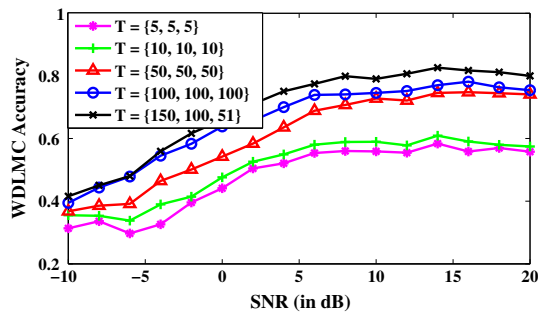
Fig. 8 Ablation study of CNN based WDLMC architecture for different values of n-taps

frequency band is vacant and $\hat{k}_n \in \{1, ..., M\}$ denotes that the nth frequency band is occupied with any one of the M modulations schemes. For performance analysis in various scenarios, $\mathbf{D_{NMC}}$ is further divided into two sections: (1)

$\mathbf{D_{NMC\_IQ}}$: Time domain IQ samples of $\hat{\mathbf{X}}_s$, and 2) $\mathbf{D_{NMC\_AP}}$: Time domain amplitude-phase samples (i.e. polar representation of IQ samples) of $\hat{\mathbf{X}}_s$. Each dataset has a shape of $N \times L \times 2$ where $L = 256$ is the number of modulated symbols. In $\mathbf{D_{NMC\_IQ}}$, the two vectors of third dimension denote in-phase and quadrature phase components of $\hat{\mathbf{X}}_s$. We normalize this dataset in the range [0,1] before passing it to the DL models. Similarly, in $\mathbf{D_{NMC\_AP}}$, amplitude and phase form two vectors of third dimension. The amplitude is normalized via l_2 norm and phase (in radians) is normalized in the range $[-1, 1]$ as in [23].

Furthermore, in each case, we consider three types of wireless channels: (1) AWGN ($\mathbf{D_{NMC\_IQ1}}$ and $\mathbf{D_{NMC\_AP1}}$), (2) AWGN channel and Rayleigh fading with a Doppler shift ($\mathbf{D_{NMC\_IQ2}}$ and $\mathbf{D_{NMC\_AP2}}$), and (3) AWGN channel and Rician fading with a Doppler shift ($\mathbf{D_{NMC\_IQ3}}$ and $\mathbf{D_{NMC\_AP3}}$).

6.3 $\mathbf{D_{WMC}}$: WDLMC dataset

The $\mathbf{D_{WMC}}$ dataset is generated directly from the complex valued reconstructed wideband signal, $\hat{\mathbf{X}}$ of size $N \times Q$. This dataset is also separated into real and imaginary parts and hence, it is of size $N \times Q \times 2$. Since the dataset classifies the modulation schemes of all N frequency bands, the dataset $\mathbf{D_{WMC}}$ has labels, $\hat{\mathbf{k}} \in \{0, 1, .., M\}$ as in $\mathbf{D_{NMC}}$. Likewise, we consider three types of wireless channels: 1) AWGN ($\mathbf{D_{WMC1}}$), 2) AWGN channel and Rayleigh fading with a Doppler shift ($\mathbf{D_{WMC2}}$), and 3) AWGN channel and Rician fading with a Doppler shift ($\mathbf{D_{WMC3}}$).

6.4 Training parameters and tools

The neural networks are implemented using Keras [46] with Tensorflow backend on Nvidia Cuda enabled Quadro P4000 GPU. The weights of the models are initialized using default Keras initializers. We use an Adam optimizer whose parameters are set as $\beta_1 = 0.9$ and $\beta_2 = 0.999$ [47].

Table 6 CNN Architecture for the proposed WDLMC

Layers	Filter size	Number of filters	Output dimension
Input			$N \times Q \times 2$
Conv/ReLu	1×150	256	$N \times 150 \times 256$
Conv/ReLu	1×100	128	$N \times 51 \times 128$
Conv/ReLu	1×51	64	$N \times 1 \times 64$
Conv/ReLU	1×1	$M+1$	$N \times 1 \times (M+1)$
Custom pool/softmax			$N \times (M+1)$

7 Performance comparison

In this section, we present results to compare the performance of the proposed architectures with the state-of-the-art works in literature. From a wireless communication perspective, we consider two parameters: (1) Spectrum sensing accuracy which in turn guarantees accurate spectrum reconstruction from SNS samples, (2) Modulation classification accuracy for a wide range of SNRs and wireless channels.

7.1 Spectrum sensing performance analysis

In Fig. 9, we compare the spectrum sensing accuracy of the proposed DLWSS architecture with conventional OMP based approach [19], which unlike DLWSS, requires the prior knowledge of the number of occupied frequency bands. The analysis is performed for three different wireless channels. As expected, DLWSS outperforms OMP at low SNRs. Furthermore, at a low SNR of -10 dB, the accuracy is 5.02%, 5.53% and 3.04% higher than OMP for AWGN, Rayleigh and Rician fading channels, respectively. Thus, as discussed in Section 4, the proposed DLWSS method, in addition to being more efficient and less computationally intensive than OMP based spectrum sensing, also improves the performance. Furthermore, switching from OMP to DLWSS based spectrum reconstruction also allows a reconfigurable architecture via a single unified pipeline due to similarity between DLWSS, NDLMC and WDLMC building blocks.

Next, we compare the execution time of the proposed DLWSS and OMP for different fractions of test data size. The OMP algorithm follows an iterative approach where it identifies an occupied band and removes its contribution from the residual matrix. This process is repeated P times (number of occupied bands) or till the stopping criterion is reached. This corresponds to P iterations in total . The proposed DLWSS, as shown in Algorithm 2, directly takes the signal $\tilde{\mathbf{X}} = \mathbf{A}^{\dagger}\mathbf{Z}$ as an input and simultaneously predicts the status of all bands in a single forward pass without the need of an iterative process. In Fig. 10, we compare the execution time of the proposed DLWSS and OMP for the different number of test samples. It can be observed that the execution time of the proposed DLWSS is significantly lower than that of OMP.

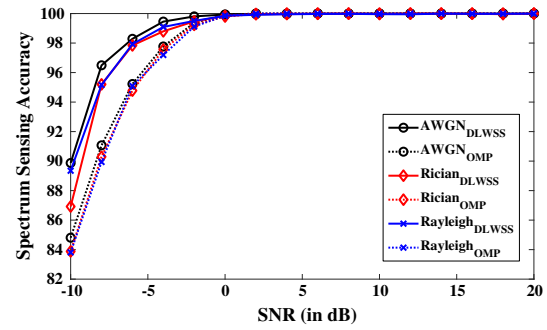To study the scalability with variable input signal dimension, we analyse the complexity of the proposed

Fig. 9 Spectrum sensing accuracy of the proposed DLWSS and existing OMP method for various channel models

DLWSS, OMP and [16–18] algorithms. Since the hyperparameters i.e. filter size, T (i.e. $\{150, 100, 51\}$), and number of filters, n_{filter} (i.e. $\{256, 128, 64\}$) and number of input signal channels $C = 2$ (i.e for real and imaginary), of the proposed 3-layer CNN based DLWSS do not vary with the change in input sizes $N \times Q$, the layer 1 requires $(N)(Q - 150 + 1) * 2 * 150 * 256 * 2$ operations[2] This corresponds to a complexity of $O(NQ)$ asymptotically. Similarly, the second and third layers also follow the same complexity. Thus, the proposed DLWSS has $O(NQ)$ complexity.

In contrast to this, the iterative OMP is divided into four steps: (1) Matching; (2) Identification; (3) Least squares step and (4) Approximation step. The approaches in [16–18] are based on the iterative procedure and involve all four steps as in OMP. But they further add a deep learning network (Convolution [16] or FC [17] or LSTM [18] networks) in the matching step. In Table 7, we compare the computation complexity of the proposed DLWSS with OMP and [16–18]. It can be observed that the proposed DLWSS has the lowest computational complexity.

7.2 Modulation classification accuracy comparison

For modulation classification, we compare the performance of the proposed NDLMC and WDLMC architectures for various IQ datasets discussed in Sect. 6. Please refer to Appendix for results on AP datasets. We consider the comparison with various approaches discussed in Section 2 such as SVM classifier with linear function kernel (P-SVM) and random forest with 10 and 150 trees in [23, 24] (P-RF10/150). Since these approaches demand Nyquist-sampled signal, we apply the proposed DLWSS based DLDR for reconstruction. Furthermore, these approaches [23, 24], cannot characterize the multiband signal directly, hence, we sequentially pass the detected occupied bands via symbol recovery compared to simultaneous

---

[2] For a convolution filter of size $1 \times T$ and input signal of size $N \times Q$ with channel C, the filter has to be convolved $(N)(Q - T + 1)$ times over the entire signal, and each convolution requires $2T$ operations.This is done for the n_{filter} number of filters i.e. $(N)(Q - T + 1) * 2T * n_{filter}C$ computations
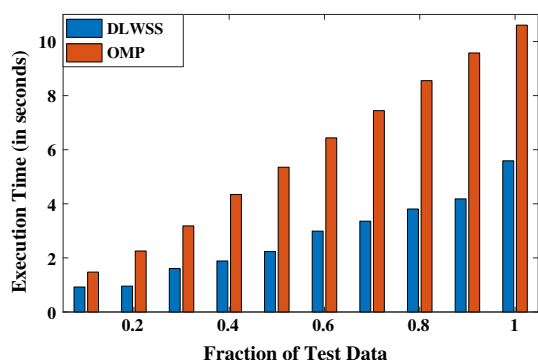
Fig. 10 Execution time comparison for proposed DLWSS framework and OMP with varying test data size

classification in the proposed approach. Thus, only occupied bands were considered while calculating modulation classification accuracy. In addition, we also considered the SVM classifier used in [15], but its performance is similar to P-RF150, and hence, it is not included in the plots. The CNN_{NS} approach in Figs. 11 and 13 are the proposed NDLMC and WDLMC applied on the symbols obtained from the Nyquist samples (NS) and directly on the wideband NS, respectively. Also, CNN_{NS} requires the prior knowledge of occupied bands [24]. In contrast, CNN_{OMP} represents NDLMC (for Fig. 11) and WDLMC (for Fig. 13), applied on the signal reconstructed via OMP instead of DLWSS. Note that the NS approach needs additional signal processing operation before classification.

7.2.1 D_{NMC_IQ}

The modulation classification accuracy of baseband converted wideband signal for AWGN, Rayleigh and Rician channels for dataset D_{NMC_IQ} are shown in Fig. 11 (a) and (b). As shown in Fig. 11 (a), for AWGN channel i.e. with a dataset D_{NMC_IQ1}, the average accuracy is 88.95% and 96.42% for SNR range of -10 dB to 20 dB and 0 dB to 20 dB, respectively. At high SNR, the accuracy of the proposed architectures is the same as NS based approaches while this is not true for $CNN_{Baseline}$ approach. As discussed

before, $CNN_{Baseline}$ also demands additional complex signal processing between reconstruction and classification stages. Next, in Fig. 11 (b), we consider the challenging Rayleigh and Rician wireless channels and corresponding classification accuracy for datasets D_{NMC_IQ2} and D_{NMC_IQ3}, respectively. Here, $Rayleigh_{NS}$ and $Rician_{NS}$ use the CNN classifier on the symbols obtained from the NS of the received wideband signal. Overall, the average accuracy for Rayleigh and Rician fading channels is 77.40% and 77.72%, respectively, along with closed match between SNS and NS approaches.

To understand the classifier performance and inter-class discrepancies better, we analyse the confusion plots of the proposed NDLMC at an SNR of 0 dB and 18 dB for all three channel models in Fig. 12. For all the channel models, at an SNR of 18 dB, we can clearly see a sharp diagonal with almost perfect classification except for 16-QAM and 64-QAM. As the SNR reduces, the sharpness of the diagonal further reduces in the 16/64/128-QAM region. Since similar observation is also valid for NS based classifier, we observed that classification of QAM schemes at low SNR is challenging and there is a scope for improvement. Nonetheless, the proposed solution offers better performance than existing state-of-the-art approaches [15, 20, 22–24] and directions for future work.

7.2.2 WDLMC

Next, we consider WDLMC scenario for the same three channels and corresponding results are shown in Fig. 13 (a) and (b) for dataset D_{WMC}. Since the classification of direct wideband signal has not been done yet in the literature, there is no baseline architecture for comparison. As shown in Fig. 13 (a), for the AWGN channel i.e. for dataset D_{WMC1}, the average accuracy is 70% and 78% for SNR range of -10 dB to 20 dB and 0 dB to 20 dB, respectively. At high SNR, accuracy of the proposed architectures is same as NS based approaches.

Classification performance of dataset D_{WMC2} and D_{WMC3} is shown in Fig. 13 (b). Here $Rayleigh_{NS}$ and $Rician_{NS}$ use CNN classifier directly on the received signal,

Table 7 Comparison of various subset learning algorithms

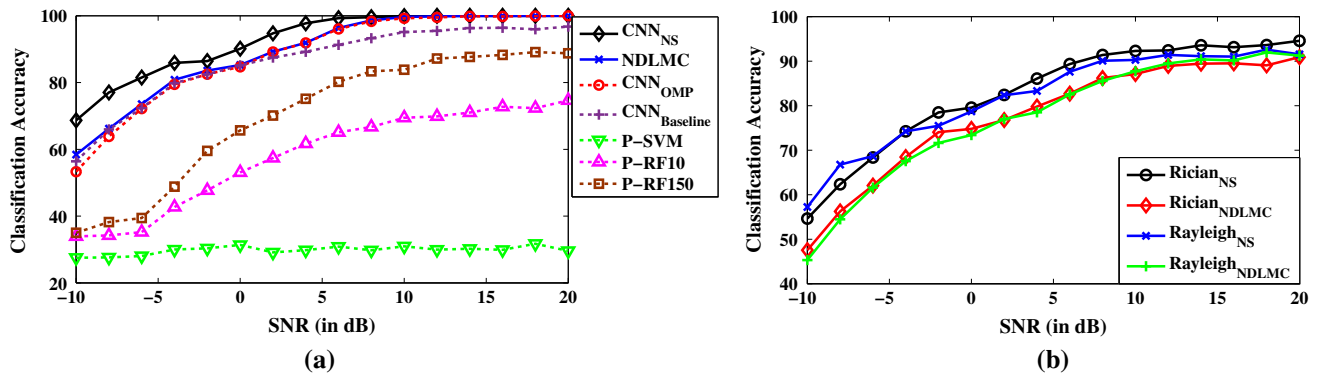| Operations	OMP	[16]	[17]	[18]	Proposed
Matching	$O(KQNP)$	–	–	–	–
DL based Matching	–	$O(KQNP)$	$O(KQP + NQP)$	$O(PQ(4K + N))$	–
Identification	$O(NQ)$	$O(NQ)$	$O(NQ)$	$O(NQ)$	–
Least Square	$O(KQP)$	$O(KQP)$	$O(KQP)$	$O(KQP)$	–
Approximation	$O(KQP)$	$O(KQP)$	$O(KQP)$	$O(KQP)$	–
DLWSS	–	–	–	–	$O(NQ)$

Fig. 11 Modulation classification accuracy of **a** NDLMC and other classification methods on the proposed AWSC for the dataset D_{NMC_IQ1} (i.e. IQ samples of AWGN channel) **b** NDLMC and NS based NDLMC on Rayleigh (i.e. dataset D_{NMC_IQ2}) and Rician (i.e. dataset D_{NMC_IQ3}) channel models
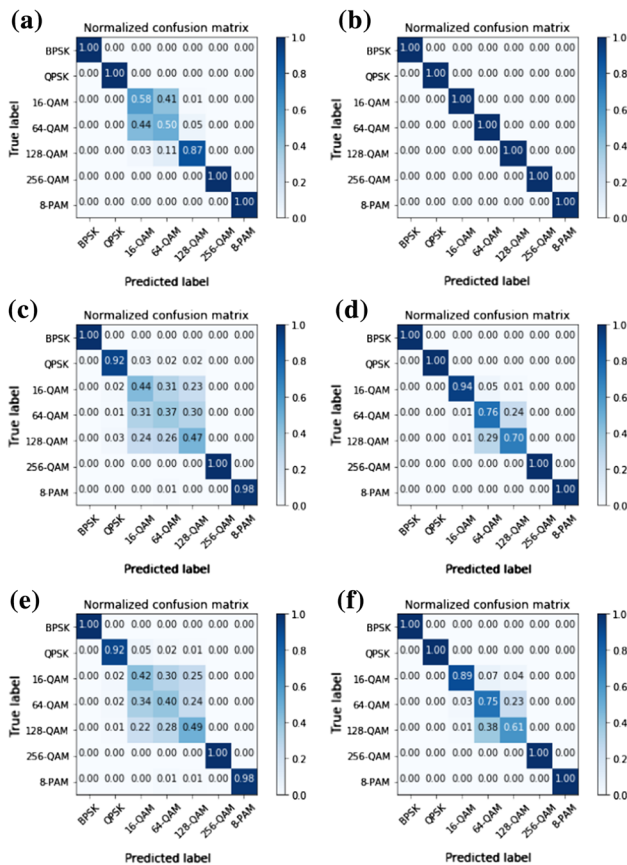

Fig. 12 Confusion plots of NDLMC on the proposed AWSC for **a** AWGN channel i.e. D_{NMC_IQ1} at SNR = 0 dB **b** AWGN channel i.e. D_{NMC_IQ1} at SNR = 18 dB **c** Rayleigh channel i.e. D_{NMC_IQ2} at SNR = 0 dB **d** Rayleigh channel i.e. D_{NMC_IQ2} at SNR = 18 dB **e** Rician channel i.e. D_{NMC_IQ3} at SNR = 0 dB **f** Rician channel i.e. D_{NMC_IQ3} at SNR = 18 dB

$x(t)$. Although the performance of the proposed SNS based WDLMC approaches to that of Nyquist sampling based DLMC (i.e. *Rayleigh$_{NS}$* and *Rician$_{NS}$*) but as expected the performance of both NS and SNS based modulation classifier is lower than the symbol based classification as shown in Fig. 11 (b). This is the small penalty incurred to reduce the complexity of additional signal processing between reconstruction and classification stages, along with making the architecture reconfigurable.

8 Conclusions and future directions

In this paper, we presented a novel deep-learning (DL) based framework for automatic wideband spectrum characterization (AWSC). We discussed the need for AWSC in next-generation networks, sub-Nyquist sampling (SNS) along with the demand of reconfigurable architecture and presented a single unified pipeline based DL architecture for SNS receivers. The proposed DL framework for AWSC performs two tasks, i.e. reconstruction of the wideband signal from the sub-Nyquist samples and automatic modulation classification (AMC). The proposed architectures are based on the in-depth study of DL frameworks along with detailed analysis over a wide range of wireless channels, signal-to-noise ratio (SNR) and modulation schemes. We not only presented a state-of-the-art architecture for conventional narrowband AWSC approach but also explored the characterization of direct wideband spectrum for the first time in the literature.

The timing and computational complexity analysis show that the proposed reconstruction approach has lower execution time and computational complexity than the existing iterative approaches. Our results highlighted that the performance of the wideband AMC approach is lower than the narrowband AMC approach, and more research works on the DL framework and SNS approach is needed. Furthermore, the characterization of direction-of-arrival, communication standard and jammer are also important areas to
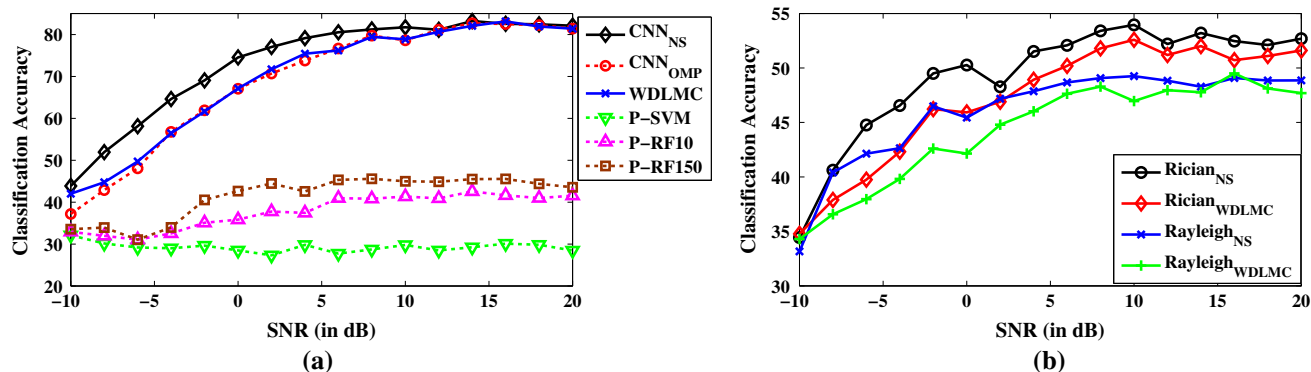
Fig. 13 Modulation classification accuracy of **a** WDLMC and other classification methods on the proposed AWSC for the dataset $\mathbf{D_{WMC1}}$ (i.e. AWGN channel) **b** WDLMC and NS based WDLMC on Rayleigh (i.e. the dataset $\mathbf{D_{WMC2}}$) and Rician (i.e. the dataset $\mathbf{D_{WMC3}}$) channel models
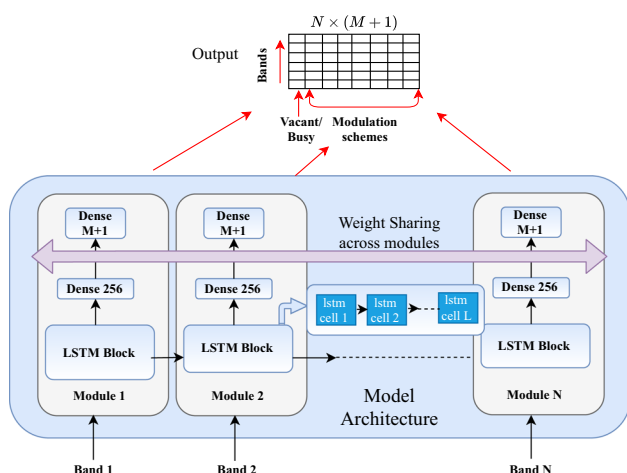

Fig. 14 LSTM architecture for NDLMC

Fig. 15 Ablation study of LSTM based NDLMC on AP samples of $\hat{\mathbf{X}}_s$

explore. Another future direction involves intelligent AWSC where additional intelligence is needed to identify the part of the spectrum to be digitized. This is important as expected operating frequency range in 5G and 6G networks is up to 60 GHz and 100 THz, respectively, and direct digitization of such wideband spectrum is challenging and inefficient. From an architecture perspective, mapping the proposed architecture to hardware, integration with SNS platform and meeting the desired latency constraints of next-generation networks are important and open research challenges.

A LSTM Architecture for NDLMC

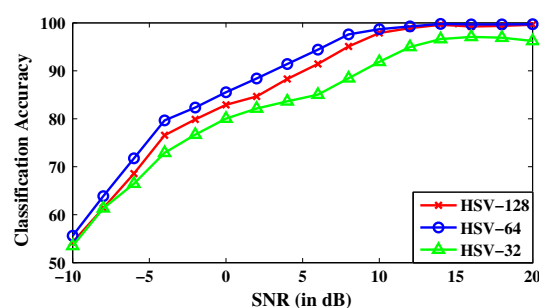Various studies in the literature have shown that the LSTM based architecture offers slightly better performance for datasets with AP samples [23]. We have also explored LSTM architecture for NDLMC and WDLMC tasks with SNS based digitization. The proposed novel architecture, shown in Fig. 14, consists of N parallel (one for each frequency band) neural network based prediction modules and these modules share the learned parameters. Note that the *LSTM block* in Fig. 14 comprises of L LSTM cells. Thus, the proposed architecture can directly process a signal of dimension $N \times L \times 2$. With reference to NS based LSTM classifier in [23], the proposed architecture can process the multi-band signal simultaneously without increasing the weight-complexity.

For this architecture, we perform the ablation study for selecting the appropriate value of hidden state vector (HSV) hyper-parameter [23]. As shown in Fig. 15, we choose HSV of 64 as it offers better performance than HSV = 32 and lower computational time than HSV = 128.

The modulation classification accuracy of the proposed NDLMC on the LSTM classifier for AWGN, Rayleigh and Rician fading channel models are shown in Fig. 16 (a) and (b). For AWGN channel with dataset $\mathbf{D_{NMC\_AP1}}$, as shown in Fig. 16 (a), the average accuracy is 87.96% and 95.83% for SNR range of -10 dB to 20 dB and 0 dB to 20 dB,
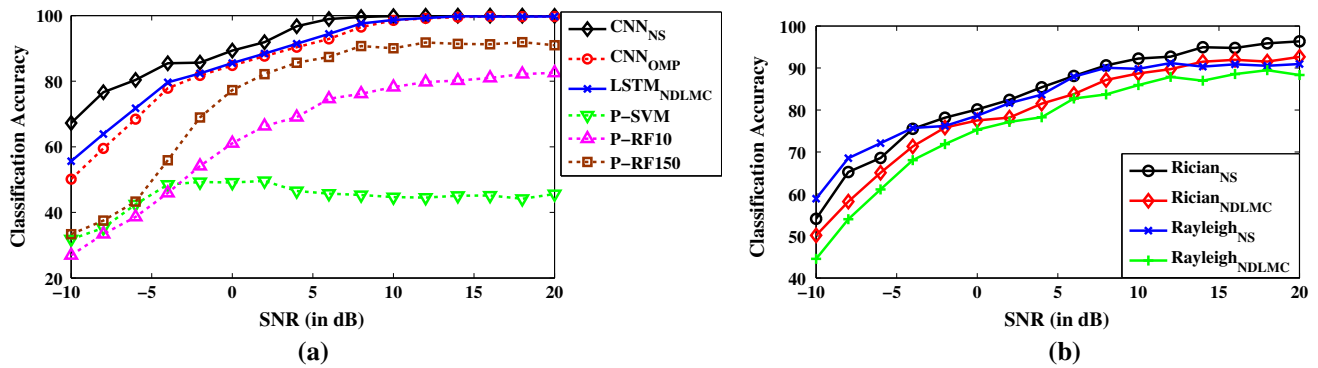
Fig. 16 Classification accuracy of LSTM based NDLMC on AP samples of **a** AWGN channel i.e. $\mathbf{D_{NMC\_AP1}}$ **b** Rayleigh channel i.e. $\mathbf{D_{NMC\_AP2}}$ and Rician channel $\mathbf{D_{NMC\_AP3}}$

Table 8 Average Classification performance Comparison of Signal recovered using proposed method

Method	AWGN	Rayleigh	Rician
NDLMC-LSTM(D_{NMC_AP1})	88	76.4	79.6
NDLMC-CNN(D_{NMC_AP1})	88.1	76.2	76.8
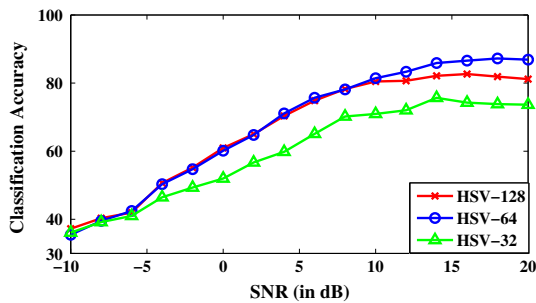
Fig. 17 Ablation study of LSTM based WDLMC on the dataset $\hat{\mathbf{X}}$ (i.e. on $\mathbf{D_{WMC1}}$)
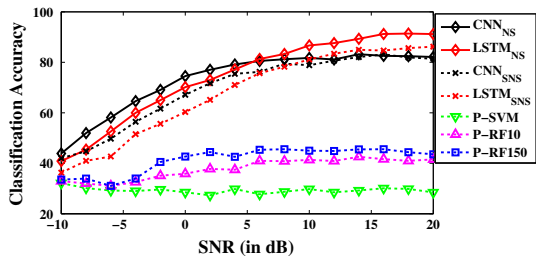

Fig. 18 Classification Accuracy of CNN based WDLMC (i.e. CNN_{NS} for Nyquist samples and CNN_{WDLMC} for SNS) and LSTM based WDLMC (i.e. $LSTM_{NS}$ fo Nyquist samples and $LSTM_{WDLMC}$ for SNS) on AWGN channel i.e. dataset $\mathbf{D_{WMC1}}$

respectively. Similar to NDLMC on the CNN classifier, at a SNR of 10 dB, its classification accuracy becomes 100%. Fig. 16 (b) shows the classification accuracy for Rayleigh and Rician fading channels i.e. for dataset $\mathbf{D_{NMC\_AP2}}$ and $\mathbf{D_{NMC\_AP3}}$, respectively. The average accuracy for Rayleigh fading channel conditions is 76.4% whereas it is 79.66% for Rician fading channel. Please note that here $Rayleigh_{NS}$ and $Rician_{NS}$ use the LSTM classifier of architecture shown in Fig. 14 on the recovered symbols $\hat{\mathbf{X}}_s$.

Table 8 shows the classification performance comparison of NDLMC when CNN classifier and LSTM classifier are used for DLMC task. It is observed that the classification accuracy of NDLMC with CNN and LSTM classifier is almost same for AWGN and Rayleigh fading channel whereas LSTM classifier performs better than CNN classifier for Rician fading channel.

B LSTM Architecture for WDLMC

We use the LSTM architecture shown in Fig. 14 for WDLMC. However, every LSTM block consists of Q LSTM cells. Thus, the architecture takes the direct wideband signal of dimension $N \times Q \times 2$ as input. We perform ablation study for the different size of HSV as shown in Fig. 17. It is found that similar to the NDLMC case, HSV=64 gives the better performance.

B.1 Performance Analysis

Next we show the classification performance comparison of LSTM with other algorithms on the reconstructed wideband signal, $\hat{\mathbf{X}}$. Here, $LSTM_{WDLMC}$ and CNN_{WDLMC} represent the performance of the LSTM and CNN, respectively, on the $\hat{\mathbf{X}}$. For the AWGN channel with dataset $\mathbf{D_{WMC1}}$, as shown in Fig. 18, the average accuracy of $LSTM_{SNS}$ is 67.7% for SNR range of -10 dB to 20 dB. Note

that the performance of the proposed CNN_{WDLMC} model is better than the $LSTM_{WDLMC}$ especially at low SNR. At very high SNR i.e above 12 dB, the performance of $LSTM_{WDLMC}$ is found to be slightly better than CNN_{WDLMC}. However, the average accuracy of $LSTM_{WDLMC}$ for SNR range of -10 dB to 20 dB (i.e 67.7%) is poorer than that of CNN_{WDLMC} model (i.e 69.5%).

To summarize, LSTM based AMC does not offer significant improvement in performance compared to CNN based AMC in case of dataset with AP samples. Furthermore, LSTM performs poorly for IQ datasets. Thus, we conclude that CNN based classifier is the preferred approach for SNS based AWSC and offers reconfigurable architecture due to similarity with DLWSS block.

Declaration

Conflict of interest Not applicable

References

1. Sengupta, S., Chatterjee M. and Ganguly S. (2007). An economic framework for spectrum allocation and service pricing with competitive wireless service providers. *IEEE International Symposium on New Frontiers in Dynamic Spectrum Access Networks (Dyspan)*.
2. Zhang, L., Xiao, M., Wu, G., Alam, M., Liang, Y., & Li, S. (2017). A survey of advanced techniques for spectrum sharing in 5G networks. *IEEE Wireless Communications, 24*(5), 44–51.
3. López, D., Rivas, E., & Gualdron, O. (2019). Primary user characterization for cognitive radio wireless networks using a neural system based on Deep Learning. *Springer Artificial Intelligence Review, 52,* 169–195.
4. Han, C., Bicen, A. O., & Akyildiz, I. F. (2015). Multi-ray channel modeling and wideband characterization for wireless communications in the Terahertz Band. *IEEE Transactions on Wireless Communications, 14*(5), 2402–2412.
5. Poisel, R. A. (2008). *Introduction to communication electronic warfare systems*. Massachusetts, United States: Artech House Inc.
6. Jeon, J. (2018). NR wide bandwidth operations. *IEEE Communications Magazine, 56*(3), 42–46.
7. Abu-Romoh, M., Aboutaleb, A., & Rezki, Z. (2018). Automatic modulation classification using moments and likelihood maximization. *IEEE Communications Letters, 22*(5), 938–941.
8. Alahmadi, A., Abdelhakim, M., Ren, J., & Li, T. (2014). Defense against primary user emulation attacks in cognitive radio networks using advanced encryption standard. *IEEE Transactions on Information Forensics and Security, 9*(5), 772–781.
9. Mishali, M., & Eldar, Y. C. (2011). Sub-nyquist sampling. *IEEE Signal Processing Magazine, 28*(6), 98–124.
10. Bagheri, S., & Scaglione, A. (2015). The restless multi-armed bandit formulation of the cognitive compressive sensing problem. *IEEE Transactions on Signal Processing, 63*(5), 1183–1198.
11. Chandhok, S., Joshi, H., Darak, S. J., and Subramanyam, A. V. (2019, January). LSTM guided modulation classification and experimental validation for sub-Nyquist rate wideband spectrum sensing. *IEEE International Conference on Communication Systems & Networks (COMSNETS)* 458-460.
12. Lim, C. W., and Wakin, M. B. (2012). Automatic modulation recognition for spectrum sensing using nonuniform compressive samples. *IEEE International Conference on Communications (ICC)* 3505-3510.
13. Zhou, L., and Man, H. (2013). Wavelet cyclic feature based automatic modulation recognition using nonuniform compressive samples. *IEEE Vehicular Technology Conference (VTC Fall)* pp. 1-6.
14. Ramjee, S., Ju, S., Yang, D., Liu, X., Gamal, A. E., and Eldar, Y. C. (2019). Fast deep learning for automatic modulation classification. arXiv preprint arXiv:1901.05850.
15. Joshi, H., Darak, S. J., & Louet, Y. (2018). Spectrum blind recovery and application in non-uniform sampling based automatic modulation classifier. *Springer Circuits, Systems, and Signal Processing, 37*(8), 3457–3486.
16. Palangi, H., Ward, R., and Deng, L. (2017). Convolutional deep stacking networks for distributed compressive sensing. *Elsevier: Signal Processing*, 131, 181-189.
17. Palangi, H., Ward, R., and Deng, L. (2013). Using deep stacking network to improve structured compressed sensing with multiple measurement vectors. *IEEE International Conference on Acoustics, Speech and Signal Processing*. 3337-3341.
18. Palangi, H., Ward, R., & Deng, L. (2016). Distributed compressive sensing: A deep learning approach. *IEEE Transactions on Signal Processing, 64*(17), 4504–4518.
19. Cai, T. T., & Wang, L. (2011). Orthogonal matching pursuit for sparse signal recovery with noise. *IEEE Transactions on Information Theory, 57*(7), 4680–4688.
20. Xu, Y., Li, D., Wang, Z., Guo, Q., & Xiang, W. (2019). A deep learning method based on convolutional neural network for automatic modulation classification of wireless signals. *Wireless Networks, 25*(7), 3735–3746.
21. O'Shea, T. J., Roy, T., & Clancy, T. C. (2018). Over-the-air deep learning based radio signal classification. *IEEE Journal of Selected Topics in Signal Processing, 12*(1), 168–179.
22. West, N. E., and O'Shea, T. (2017). Deep architectures for modulation recognition. *IEEE International Symposium on Dynamic Spectrum Access Networks (DySPAN)*, 1-6.
23. Rajendran, S., Meert, W., Giustiniano, D., Lenders, V., & Pollin, S. (2018). Deep learning models for wireless signal classification with distributed low-cost spectrum sensors. *IEEE Transactions on Cognitive Communications and Networking, 4*(3), 433–445.
24. O'Shea, T. J., Corgan, J., and Clancy, T. C. (2016). Convolutional radio modulation recognition networks. *Springer Engineering Applications of Neural Networks (EANN)*. 213-226.
25. https://drive.google.com/drive/folders/1uAzu-RbNNMu38SLnMLS77Vf75DuW17RZ?usp=sharing
26. Marques, E. C., Maciel, N., Naviner, L., Cai, H., & Yang, J. (2018). A review of sparse recovery algorithms. *IEEE Access, 7,* 1300–1322.
27. Blanchard, J. D., Cermak, M., Hanle, D., & Jing, Y. (2014). Greedy algorithms for joint sparse recovery. *IEEE Transactions on Signal Processing, 62*(7), 1694–1704.
28. Blanchard, J. D., Cermak, M., Hanle, D., & Jing, Y. (2014). Greedy algorithms for joint sparse recovery. *IEEE Transactions on Signal Processing, 62*(7), 1694–1704.

29. Mota, J. F., Xavier, J. M., Aguiar, P. M., & Puschel, M. (2011). Distributed basis pursuit. *IEEE Transactions on Signal Processing, 60*(4), 1942–1956.

30. Yucek, T., & Arslan, H. (2009). A survey of spectrum sensing algorithms for cognitive radio applications. *IEEE Communications Surveys and Tutorials, 11*(1), 116–130.

31. Lavate, T. B., Kokate, V. K., and Sapkal, A. M. (2010). Performance analysis of MUSIC and ESPRIT DOA estimation algorithms for adaptive array smart antenna in mobile communication. *IEEE Second International Conference on Computer and Network Technology*. 308-311.

32. Azzouz, E., and Nandi, A. K. (2013). *Automatic modulation recognition of communication signals*. Springer Science & Business Media.

33. Lin, Y., Tu, Y., Dou, Z., Chen, L., & Mao, S. (2021). Contour stella image and deep learning for signal recognition in the physical layer. *IEEE Transactions on Cognitive Communications and Networking., 7*(1), 34–46.

34. Wang, Y., et al. (2020). Distributed learning for automatic modulation classification in edge devices. *IEEE Wireless Communications Letters, 9*(12), 2177–2181.

35. Wang, Y., Gui, G., Ohtsuki, T. and Adachi, F. (2021). Multi-task learning for generalized automatic modulation classification under non-gaussian noise with varying SNR conditions. *IEEE Transactions on Wireless Communications*.

36. O'Shea, T. J., Roy, J., and Clancy, T. C. (2018). https://www.deepsig.io/datasets

37. Ioushua, S. S., Yair, O., Cohen, D., & Eldar, Y. C. (2017). CaSCADE: Compressed carrier and DOA estimation. *IEEE Transactions on Signal Processing, 65*(10), 2645–2658.

38. Kumar A. A., Razul S. G., and See C. M. S. (2014). "An efficient sub-Nyquist receiver architecture for spectrum blind reconstruction and direction of arrival estimation, " in *IEEE International Conference on Acoustics, Speech and Signal Processing*, pp. 6781-6785, Florence, Italy.

39. Kumar, A. A., Razul, S. G., and See, C. M. S. (2014). An efficient sub-Nyquist receiver architecture for spectrum blind reconstruction and direction of arrival estimation. *IEEE International Conference on Acoustics, Speech and Signal Processing (ICASSP)*. 6781-6785.

40. Mishali, M., Eldar, Y. C., Dounaevsky, O., & Shoshan, E. (2011). Xampling: Analog to digital at sub-Nyquist rates. *IET Circuits, Devices and Systems, 5*(1), 8–20.

41. Peng, S., Jiang, H., Wang, H., Alwageed, H., Zhou, Y., Sebdani, M. M., & Yao, Y. D. (2018). Modulation classification based on signal constellation diagrams and deep learning. *IEEE Transactions on Neural Networks and Learning Systems, 30*(3), 718–727.

42. Lin, M., Chen, Q., and Yan, S. (2013). Network in network. arXiv preprint arXiv:1312.4400.

43. Szegedy, C., Liu, W., Jia, Y., Sermanet, P., Reed, S., Anguelov, D., and Rabinovich, A. (2015). Going deeper with convolutions. *IEEE conference on computer vision and pattern recognition*. pp. 1-9.

44. He, K., Zhang, X., Ren, S., and Sun, J. (2016). Deep residual learning for image recognition. *IEEE conference on computer vision and pattern recognition*. pp. 770-778.

45. Huang, G., Liu, Z., Van Der Maaten, L., and Weinberger, K. Q. (2017). Densely connected convolutional networks. *IEEE conference on computer vision and pattern recognition*. pp. 4700-4708.

46. Chollet, F. (2015). Keras, https://github.com/fchollet/keras .

47. Kingma, D. P., and Ba, J. (2014). Adam: A method for stochastic optimization. arXiv preprint arXiv:1412.6980.

Shivam Chandhok received the B.Tech. degree in electronics and telecommunications engineering from Jamia Milia Islamia, Delhi, India, in 2019. He is currently a Research Assistant at Indian Institute of Technology Hyderabad, Telangana, India. His research interests include Deep Learning and it's applications in the field of Computer Vision.

Himani Joshi received the B.Tech. degree in electronics and telecommunications engineering from Guru Gobind Singh Indraprastha University, Delhi, India, in 2013, and the M.Tech. degree, in 2016, from the Indraprastha Institute of Information Technology, Delhi (IIIT-Delhi), Delhi, India, where she is currently working toward the Ph.D. degree. Her current research interests include the subNyquist sampling for reconfigurable wideband receiver and hardware implementation of reconfigurable receiver for wideband signal processing.

A. V. Subramanyam received the bachelor's degree from the Indian School of Mines University, Dhanbad, India, and the Ph.D. degree from Nanyang Technological University, Singapore. He is currently an Assistant Professor at Indraprastha Institute of Information Technology, Delhi, India. His research interests include multimedia security, information hiding and forensics, person reidentification, and visual tracking.

Sumit J. Darak received his Bachelor of Engineering (B.E.) degree in Electronics and Telecommunications Engineering from Pune University, India in 2007, and Ph.D degree from the School of Computer Engineering, Nanyang Technological University (NTU), Singapore in 2013. He is currently an Assistant Professor at Indraprastha Institute of Information Technology, Delhi, India. Prior to that, he was working as Assistant System Engineer in Tata Consultancy Services (TCS), Pune, India from September 2007 to December 2008. From August 2011 to November 2011, he was visiting research student at Massey University, Auckland, New Zealand. From August 2012 to January 2013, he worked as an intern at EADS Innovation Works (Airbus), Singapore. From March 2013 to November 2014, he was pursuing postdoctoral research at the CominLabs Excellence Center, Université Europèenne de Bretagne (UEB) and Supélec, Rennes, France for the project GREAT: Green Cognitive Radio for Energy-Aware Wireless Communication Technologies Evolution. Dr. Sumit has been awarded India Government's 'DST Inspire Faculty Award' which is a prestigious award for young researchers under 32 years age. His research interests include design and implementation of multistandard wireless communication receivers as well as application of machine learning algorithms and decision making policies for various wireless communication applications.